CHARACTERIZATION OF SEMICONDUCTOR AND FRONTIER MATERIALS BY NUCLEAR MICROPROBE TECHNOLOGY

Jieqing ZHU, Xiaolin LI, Changyi YANG, Rongrong LU, Jiqing WANG, Panlin GUO
Shanghai Institute of Nuclear Research,
Chinese Academy of Sciences,
Shanghai, China

Abstract

The nuclear microprobe technology is used to characterize the properties of semiconductor and other frontier materials at the stages of their synthesis, modification, integration and application. On the basis of the beam current being used, the analytical nuclear microprobe techniques being used in this project can be divided into two categories: high beam current (PIXE, RBS, PEB) or low beam current (IBIC, STIM) techniques. The material properties measured are the thickness and composition of a composite surface on a SiC ceramic, the sputtering-induced surface segregation and depth profile change in a Ag-Cu binary alloy, the irradiation effects on the CCE of CVD diamond, the CCE profile at a polycrystalline CVD diamond film and a GaAs diode at different voltage biases and finally, the characterization of individual sample on an integrated material chip.

1. Introduction

Many aspects of modern technology depend on the development of semiconductor and other frontier materials that have unique properties. The quality of the materials must be controlled at all the stages in the process of the material development: synthesis, modification, integration and eventual application. MeV ion beam analysis has been widely used to characterize surface properties of materials. Surfaces of many materials are composed of small (μm) grains, crystals and different phase regions. The nuclear microprobe with a reasonable spatial resolution (μm) is suitable to probe these small regions for their composition and structure and to profile their depth distribution.

By means of the nuclear microprobe at SINR and in cooperation with other two CRP groups (University of Torino, Italy and Rudjer Boskovic Institute, Croatia), we have measured the properties of some semiconductor and other frontier materials. They are nitride surface on SiC ceramic, Ag-Cu binary alloy surface, CVD diamond film, GaAs detector, and finally combinatorial material chips. On the basis of the beam current being used, the analytical nuclear microprobe techniques being used in this project can be divided into two categories: high beam current (PIXE, RBS, PEB) or low beam current (IBIC, STIM) techniques.

The mechanical strength of silicon carbide ceramic (SiC) can be much improved by formation of a composite ceramic layer on its surface. The micro-PEB (proton elastic backscattering) technique was used to study the composite ceramic layer (Si_3N_4) made by exposing SiC to N_2 atmosphere at high temperature. The nitride surface results in a remarkable increase of the material strength. The improved properties of the ceramic are dominated by the Si_3N_4 concentration in the composite layer, but not by the layer thickness.

Preferential sputtering-induced surface segregation and localized depth profile change in a Ag-Cu binary alloy was studied by micro-PIXE and micro-RBS. The ion sputtering was performed by Ar^+ beam bombardment. Pronounced changes of the surface concentration and the depth profile have been found at both Cu-enriched solid solution micro-grains and Ag-enriched matrix regions. The bombardment-induced segregation is suggested to be attributed to the composition change in the very near surface region.

Lateral micro-IBIC was used to characterize the electrical behavior of CVD diamond thin film and further to evaluate its quality. By comparing the IBIC results between samples of non-irradiated and irradiated with proton dose of 46 Gy, we found that the average charge collection distance of the diamond film was obviously increased due to the fact that the space charge inside the film was eliminated by irradiation. The change of charge collection efficiency (CCE) at different biases applied on the growth side of the CVD diamond film was investigated by lateral micro-IBIC. The responsibility of the internal electric field for the change was theoretically studied. It was confirmed that the CVD diamond film was similar to a reverse biased p-n junction. Electrons were main contributors to

CCE while holes had high trapping probability in the diamond film. The CCE distribution in a GaAs diode was measured by frontal micro-IBIC technique. The IBIC image produced by helium ion beam had better contrast than that by proton beam because helium ion deposited more energy in the depletion layer of the diode.

We have developed a method combining ion implantation and physical masking technique to generate a material library of various ion-implanted samples. Six ion species have been sequentially implanted to a SiO_2 film through six combinatorial masks and consequently a material chip (library) with 64 (2^6) samples is generated. RBS and PEB are first applied for characterization of the material chip to determine the depth-resolved ion distribution in the individual sample. It is revealed by the spectrum for co-implanted sample S(Ga, C) that C existence induces the redistribution of Ga in SiO_2 after thermal annealing. It also showed that Sn diffusion approaching the surface for sample S(Pb, Sn, N) is evident, which is a cause of high luminescent emission for this material. The successful combination of ion beam implantation and ion beam analysis greatly increases the efficiency for new material synthesis, analysis and optimization.

The nuclear microprobe at SINR was initially set up for preference of micro-PIXE only. In order to conduct this project, some modification has been adopted and it is described in the first paragraph.

2. Modification of the experimental facilities for this project

The nuclear microprobe at SINR (Shanghai Institute of Nuclear Research) has been able to focus MeV protons or helium ions down to a size of one micron. The microprobe features itself with long focus quadruple lenses, and hence, it obtains good spatial resolution with easy operation. However, it was initially set up for preference of particle-induced X-ray emission (PIXE) experiments only. Before conducting this project, this microprobe has been used for mapping elemental micro-distribution of minerals and biological samples by means of micro-PIXE technique.

The nuclear microprobe has shown its potentialities in applications to semiconductor and some other frontier materials. In order to meet more demands from semiconductor and material science, some new IBA techniques have been developed with the microprobe. As complementary of PIXE, Rutherford backscattering spectrometry (RBS) is useful technique for quantitative measurement of elemental concentration profiles and ionic transport within materials. RBS-channeling can be used to study the micro-structure in crystal materials. Nuclear microprobe technique has been extended to scanning transmission ion microscopy (STIM) to measure the mass thickness of film materials. A system for ion beam induced luminescence (IBIL) and ion beam induced charge (IBIC) measurement has been installed for study of semiconductor materials and microelectronics samples.

Because the beam current of the microprobe is much lower than the ordinary IBA requests, the experiment efficiency is important. A multi-detector system around the microprobe specimen chamber makes it possible to measure a sample with some IBA techniques simultaneously. Different IBA measurement gives out different properties of a specimen. The complex microprobe measurement does much enhance the understanding of the microscopic properties of the specimen from different aspects. In order to cope with the complex microprobe measurements, a multi-detector and multi-parameter data acquisition system is built up successfully in this laboratory.

The new data acquisition system is based on the concept of TQSA (total quantitative scanning analysis) and works by a list mode. It provides the recording of all information associated with a detected data event (e.g. the detected secondary particle energy and the focused beam position). At this mode, no information is lost and the spectra or the distribution maps within any preferential areas or energy windows may be extracted on-line or at any later time. We have implemented the concept of TQSA by designing a digitized beam scanning system and a high-speed data acquisition interface FDAC (fast data acquisition crate). The FDAC provides a modular interface between the Motorola VME data acquisition computer and the scan system and ADC. The data acquisition hardware is described in Fig.1. The VME computer is connected by an ethernet link to an Unix workstation running the X-windows graphical environment. This workstation runs the MPSYS software package. It presents a high level graphical environment for on-line and off-line data treatment for the microprobe experiment. The FDAC has four stations connected to different detector systems. Each of them is triggered by events accepted by a corresponding detector. Up to four different detectors, and hence, four different IBA techniques can work simultaneously in one scanning experiment with the TQSA protocol.

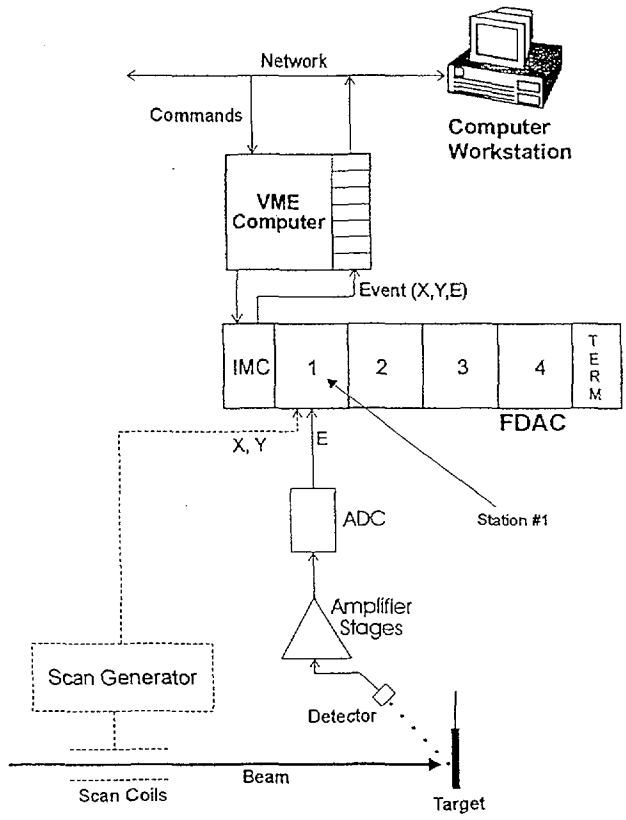

Fig.1. Schematic diagram of the general operation of the new multi-detector and multi-parameter data system hardware with a single detector providing input as a station example.

Some modifications of the microprobe for application to material science have also been made. A new pair of pre-lenses magnetic scanning coils enlarges the scanning area from the ordinary 500 mμ by 500 mμ to a new area of 2 mm by 2 mm for 3 MeV proton beam. An universal specimen holder is designed for holding several thick and large samples easily. The specimen holder can be moved along three directions and rotated in two axes with large movement ranges. The illumination in the specimen chamber is improved and a side window is attached at the chamber to have better viewing. A pair of X-ray filters is put in front of the Si(Li) detector. It can be moved without the necessity to open the chamber. A small area surface barrier detector with good energy resolution is installed at 135° direction for RBS and channeling experiments. An annular surface barrier detector is installed in front of the sample for light element detection and sample matrix measurement. An off-axis STIM measuring detector is installed at 5° direction, which can be changed from outside the vacuum chamber.

The high current microprobe techniques typically employ beam current in excess of 50 pA focused into a spot of ≥2 μm. The beam current for the low current techniques is typically smaller than that of the high current techniques by a few orders of magnitude. The difficulty for the low current technique is how to produce a low current beam without deteriorating the beam spot resolution. We mount a sample for low current experiment and a piece of glass together on a specimen holder. At first, we focus the ion beam with high beam current while it hits on the glass. The beam spot size and position are measured with a high power optical microscope. The beam position is marked by cross hairs in the view field of the microscope. After that we close down the object slits to 5 μm and adjust the velocity selector of the accelerator to reduce the beam intensity at a level of 500 ions/s. Then, the sample is moved to the marked position by two-dimensional displacement of the specimen holder.

For IBIC measurement we firstly used an ordinary charge sensitive preamplifier which was attached at the outside of the specimen chamber. It transformed the ion-induced charge in the sample into pulse signal. Because of the long distance between the preamplifier and the sample, the electric

noise was not satisfied for high-resolution IBIC measurement. In order to achieve an adequate signal/noise ratio this distance is shortened by moving the first FET of the preamplifier into the specimen chamber. The FET is attached at the specimen holder. The FET capacitance, and hence, the noise are low and unchanged when the sample is moving.

3. Micro-analysis of Si_3N_4/SiC ceramic composite layer by micro-PEB technique

Silicon carbide, one of the high performance ceramic has been widely used in high-temperature structure applications. However, SiC is a relative brittle material. There are pores, cracks and some low density areas in sintered SiC ceramic, which limits its mechanical properties. Taking pre-sintered SiC as substrate, a technology of HIP (hot isostatic pressing) has been developed to form a layer of Si_3N_4/SiC composite ceramic on its surface. The composite layer is generated on the surface of SiC by exposing it in N_2 atmosphere at different temperatures (1850, 1900 or 2000 ^oC) for a different period of 0.5, 1 or 2 hours [1]. The physical and mechanical properties of the new product are distinctly improved. Are the improved properties dependent on the thickness and the Si_3N_4 concentration in the composite layer? The thickness and the concentration are measured with the non-Rutherford proton elastic backscattering (PEB) technique by means of a focused proton microbeam scanning across the layer.

Because the thickness of nitride layer is only slightly larger than the beam size, the sample surface was polished in a slope of 1^o crossing the original target surface and the nitride layer to improve the depth resolution. The thickness of the composite layers and their concentration of Si_3N_4 (as atomic ratio of N/C) in the layers have been determined with this technique and correlated with the HIP processing conditions and the properties of the new materials. And than the processing conditions can be optimized with the results of the microprobe analysis.

The experimental setup and a result are shown in Fig. 2. The scattered protons are detected at 170^o by an annular barrier detector. The concentration of Si_3N_4 is about 0.89 on the surface of the nitride layer and sharply decreases to 0.40 at a depth of 1 μm, and then gradually decreases until a sudden drop at a depth about 17 μm from the surface. The distance scale from the surface along the slope is also indicated in Fig. 2 for comparison. The distribution profiles of C and N concentrations along the slope in the composite layer are shown in Fig. 3. There is an interface between the SiC substrate (right) and the nitride surface (left). In considering of the oblique angle, the thickness of the interface is measured as 14 μm. It is showed that the improved properties of the ceramic are dominated by the Si_3N_4 concentration in the composite layer, but not by the layer thickness.

4. Study of localized depth distribution in a binary alloy surface after bombardment by Ar ion

It is known that some binary alloys are composed of micro-regions with different grain phases and different metal enrichment [2]. Preferential sputtering induced surface segregation and depth profile change in an alloy system is an interesting topic [3]. The surface topography is usually studied by Auger electron spectroscopy (AES) and secondary ion mass spectroscopy (SIMS). However, these methods use stripping of atoms from the target surface by ion sputtering. As a result, the atomic compositions are changed during this analysis due to ion bombardment. Rutherford backscattering (RBS) in conjunction with a microbeam technique is a nondestructive method suitable for localized depth distribution analysis.

The Ag-Cu alloy was used in this work. It contains 37% Ag by atoms. The ion sputtering was performed by bombardment of 27 KeV Ar^+ beam with a flux of $1 \times 10^{17}/cm^2$. After the Ar ion bombardment the sputtered surface of the sample was observed by electron microscope. We saw that a lot of islanded grains on a strongly textured matrix. The size of the grains was about 10 μm. According to the results of micro-PIXE analysis, the islanded grains were enriched with Cu and the matrix was enriched with Ag. The depth profiles of Cu and Ag in different regions were investigated by micro-RBS. A beam of 2 MeV He^+ ions was focused to 4 μm in diameter with a current of 1 nA. The depth profiles were determined in both of the Ar^+ bombarded area and the unbombarded area for comparison. The results revealed the sputtering induced surface segregation and the profile changes.

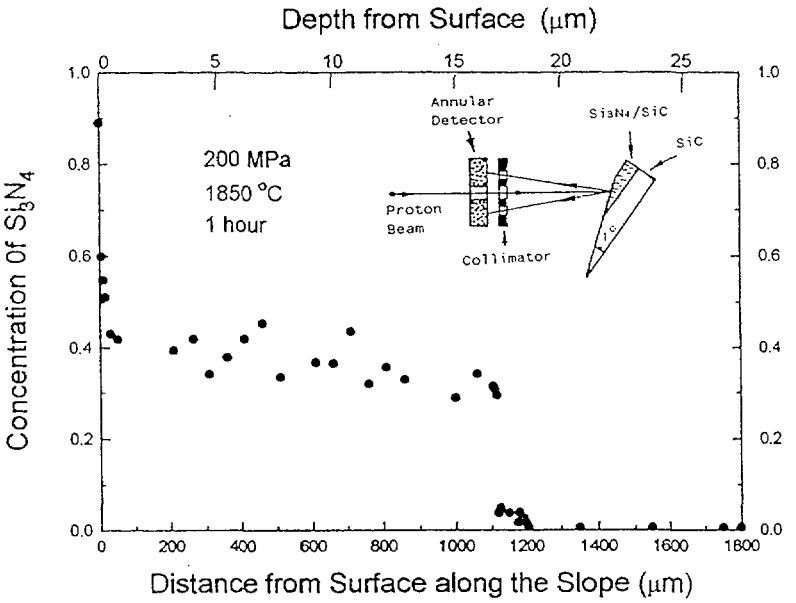

Fig. 2. Depth distribution of Si_3N_4 molecular concentration in a layer of Si_3N_4/SiC composite ceramic on the silicon carbide surface. A diagram of the experimental setup is also displayed in the figure.

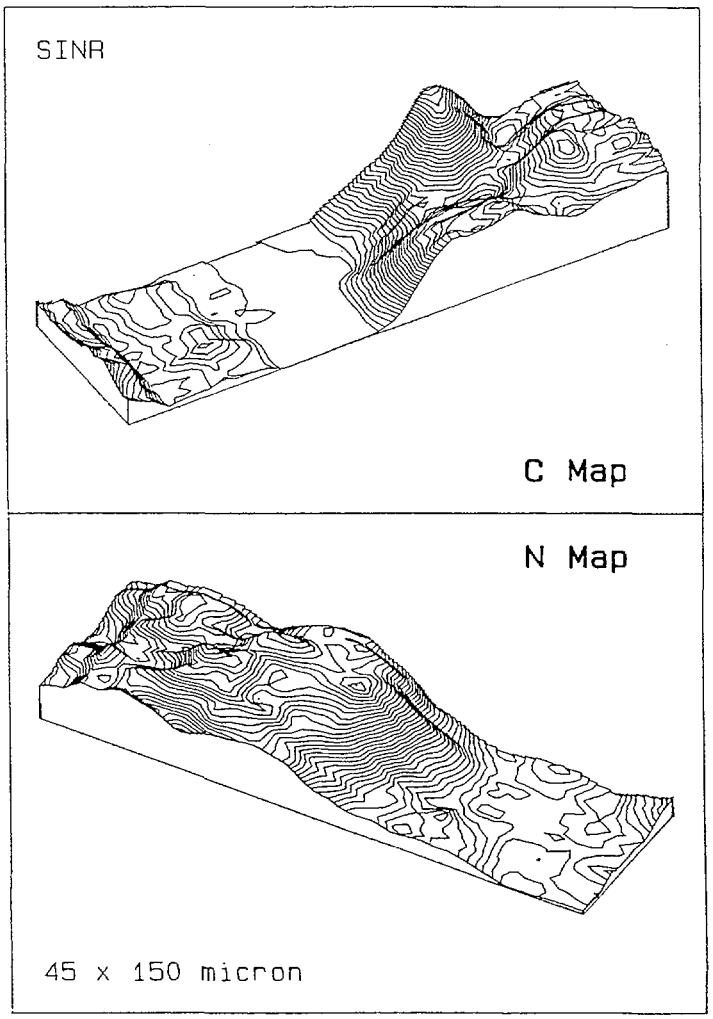

Fig. 3. 3-D contour maps for the distribution profiles of C and N concentration along the slope in a layer of Si_3N_4/SiC composite ceramic.

Fig. 4 shows the Ag concentration depth profile at the Cu enriched micro-grains. The local bulk composition of Ag is about 6.5% before bombardment at these regions. It is in good agreement with the estimated solid solubility of Ag in metal Cu by a phase diagram of Ag-Cu binary alloy. The bombarded curve in Fig. 4 indicates that Ag is relatively enriched in the outermost surface, and sharply decreases to a minimum at a depth of about a few nm from the surface, then increase slowly. This phenomenon, that the Ag solute becomes relatively enriched at the very surface and is depleted in the subsurface at the Cu-enriched solid solution regions, strongly suggests the presence of a sputtering induced Gibbsian segregation (BIGS) effect [4]. The segregation ratio is about 1.3. The Ag concentration depth profile for Ag-enriched matrix region is shown in Fig. 5. A pronounced depletion of Ag is found in the near surface region of the Ag-enriched matrix due to preferential sputtering of Ag under ion bombardment, which is the dominant factor forming the surface topography as described above. No enrichment of Ag is observed in the outermost surface layer.

5. Characterization of chemical vapor deposition (CVD) diamond and GaAs semiconductor detector by ion beam induced charge (IBIC) collection technique

This program was conducted under cooperation with other two CRP groups: University of Torino (Italy) and Rudjer Boskovic Institute (Croatia). The CVD and GaAs samples were prepared at Torino. The nuclear microprobes in Rudjer Boskovic Institute and Shanghai Institute were used for the IBIC experiments.

5.1. Study of irradiation effects on the charge collection efficiency (CCE) of CVD diamond films

Diamond has superlative electrical and structural properties for use in microelectronic devices and radiation hard detectors in high counting rate and high radiation environments including high energy physics experiments. Currently available CVD diamond allows the practical and cost-effective realization of such devices. The quality of CVD diamond is apprised by the collection length d_c, which is the average distance that electron-hole pairs drift apart before being trapped. Usually, the frontal IBIC technique is used to measure the collection length according to a simple linear relation between collection length and the thickness of the diamond film. It is valid only when the collection length is smaller than the thickness of the film. In order to characterize the electrical behavior and further to evaluate the quality of CVD diamond with longer collection length, the lateral micro-IBIC technique was used. A 200 μm thick CVD diamond sample, clamped with two Ti/Au electrodes on both of the growth and the substrate sides, was studied by introducing a 4 MeV proton beam with 4 μm beam size and very low beam current hitting at the lateral cross section of the sample. The electrode on the growth side was added by a fixed bias and the other side referenced to the ground. In the diamond film, the charged carriers were created by the proton beam. The charge pulses, generated by the motion of the charged carriers towards the electrodes due to the presence of the applied electric field, were amplified and recorded by the charge sensitive preamplifier. To evaluate the CCE and the d_c, the pulse heights were normalized to the response of a Si surface barrier detector (nominal 100% CCE) on the basis that the energy for creating a electron-hole pair is 3.6 eV in silicon and 13.2 eV in diamond.

In order to study the irradiation effects on the CCE of CVD diamond, a non-irradiated sample was firstly measured by micro-IBIC. Then, the sample was irradiated by high dose of proton beam (46 Gy) and IBIC was measured on the same area. The measured area was divided into 128 columns along the lateral cross section and the CCE in each column was calculated based on the average IBIC intensity in it. By comparing the IBIC results of non-irradiated samples with those of irradiated ones, it was found that the CCE uniformity of CVD diamond could be much increased by the irradiation. It might be due to the elimination of space charges inside the CVD diamond after irradiation. Fig. 6 shows a diagram of the column numbers at certain CCE intervals versus CCE for the non-irradiated and irradiated sample. It is of interest to note that the curve for the non-irradiated case can be fitted by a continuous line with two Gaussian curves. The curve for the irradiated case can be fitted by one Gaussian curve. The result means that the CCE profile for the non-irradiated sample is a convolution of a low CCE (0.15) part and a high CCE (0.29) part. While for the irradiated sample the high CCE (0.29) dominates the CCE profile. The low CCE part is contributed by the space charge existence in the grain boundary. The process of irradiation can eliminate the cloud of the space charge. This study provides a possibility to effectively improve the electric properties of CVD diamond semiconductors.

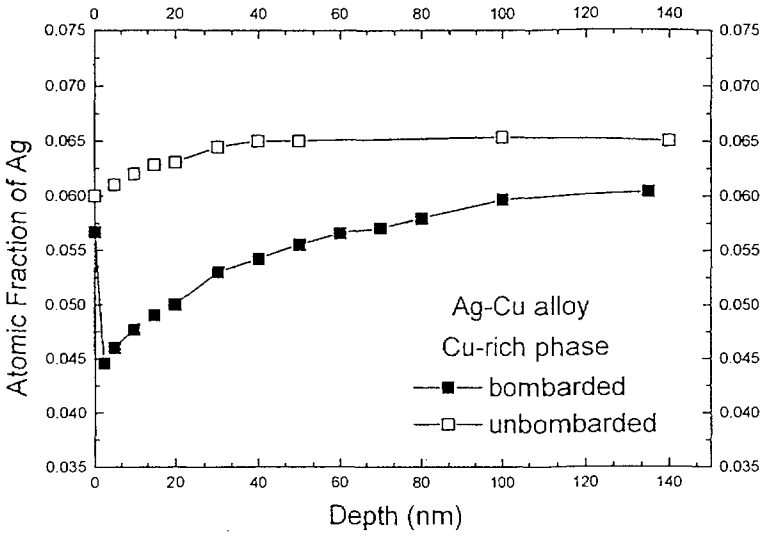

Fig. 4. Depth distribution of Ag at a Cu-enriched micro-grain on the surface of Ag-Cu alloy.

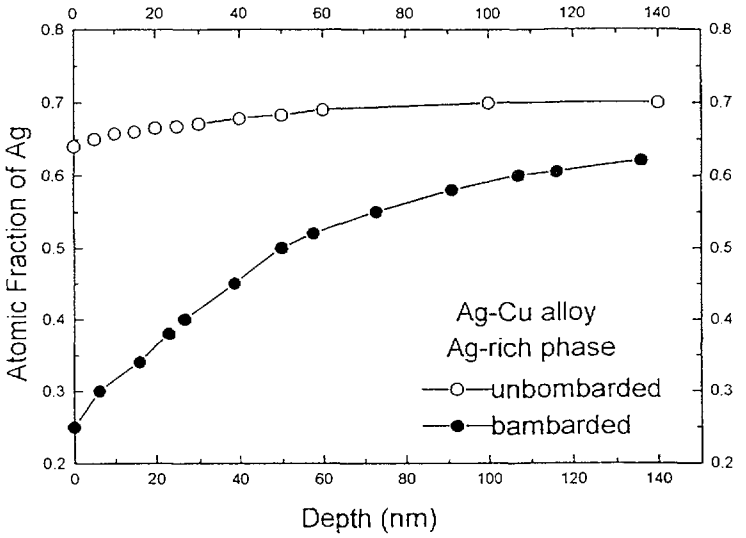

Fig. 5. Depth distribution of Ag at a micro-region of the Ag-enriched matrix on the surface of Ag-Cu alloy.

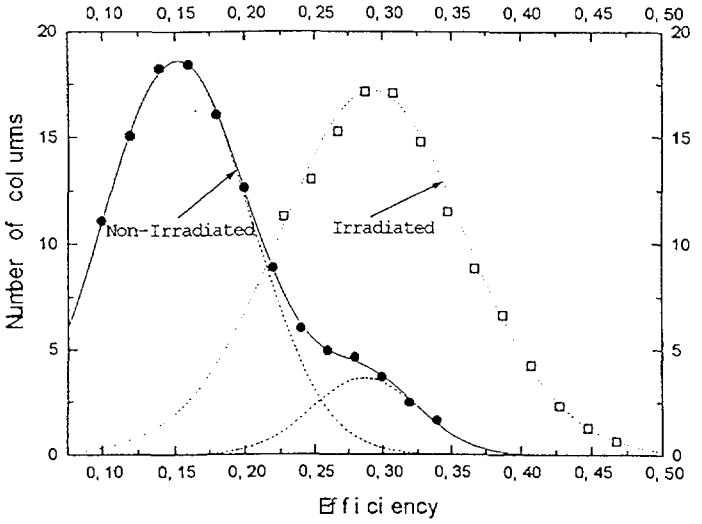

Fig.6. A diagram of the column number at certain interval of charge collection efficiency (CCE) versus CCE for the non-irradiated or irradiated sample.

5.2. Comparison of CCE profiles of polycrystalline CVD diamond film at different voltage biases

CVD diamond is polycrystalline material with columnar structure along the growth direction. This characteristic may affect the electric properties of the material by acting as traps and/or recombination centers, thus degrading its charge collection efficiency (CCE), which is defined as the ratio between the collected and the created charges or numbers of the electron-hole pairs. The information about the electric behaviors of carriers' movements inside the diamond was investigated by the micro-IBIC technique. The dependence of CCE upon the crystalline grain sizes was studied by mapping the IBIC images at different voltage biases. IBIC maps of CCE distributions in the scanning areas were obtained by means of the setting of different windows in IBIC spectrum similar to the process of PIXE elemental maps. The CCE profile along the diamond growth direction can be easily got by averaging the efficiencies in the direction normal to the growth direction. In order to get insight into the electrical and transport properties of charge carries excited by proton beam in diamond, the contributions of electrons and holes to the CCE profile are separately considered.

An extensive investigation on the electrical and transport behaviors of CVD diamond has been made by lateral micro-IBIC. The focused proton beam was scanned over an area of 200 × 500 μm^2 of a 200 μm thick CVD diamond film. The film was carefully cleaved and clamped with two electrodes on both the growth and the substrate sides. The electrode on the growth side was added by different biases and another side referenced to the ground. Fig. 7(a) shows a typical profile of CCE along the growth direction. Here, the growth side (biased) is on the left and the substrate side (ground) is on the right. It is noted that the CCE profile moves to the growth side with the increase of positive bias voltage from 400 to 600 V. The CCE maximum changes between 25 and 35% in the middle of the film. In the same way, the CCE profiles for different negative biases were obtained and displayed in Fig. 7(b). It is also noted that the highest CCE exists in the layer of growth side with a variation from 42 to 50%. The shape of the CCE profile slightly moves to the substrate side while the negative bias changes from -100 to -400 V. It was concluded that the CVD diamond film is similar to a p-n junction with a reverse bias when a positive voltage applied at the growth side. The electrons are usually the main contributors to CCE while the holes have higher trapping probability in the CVD diamond film. In the case of negative bias, the negative space charge on the growth region may come from the donors of the film and the positive space charge on the substrate region may arise from the acceptors of the film. The neutralization effect is mainly responsible for the elimination of the space charge in the middle of both electrodes.

5.3. Micro-IBIC characterization of GaAs semiconductor detector using proton beam or helium ion beam

GaAs is good semiconductor materials for making micro-electronic devices and radiation detectors. It has potential applications for the manufacture of devices working at high temperature and high power. Because of its high electron mobility, it is wildly used in high frequency and high speed circuits. Schottky barriers are generally needed in order to get low leakage currents. The properties of the devices and the energy resolution of the detectors are much of dependence on the electrical homogeneity of the GaAs materials. The CCE distribution in a GaAs diode was measured by the frontal micro-IBIC technique. The charge was collected by the electrodes at the top and the end of the diode. The resister rate of the GaAs material is 10^7 Ωcm and the life-time of the carriers is at a level of ns. The thickness of the GaAs chip is 220 μm. The Schottky barrier is formed between a top layer of Au/Pt/Ti and the GaAs material. The substrate copper layer forms the other electrode of the diode. Data were collected by two-station list model for PIXE and IBIC experiments. Both of the 3 MeV proton beam and 2 MeV helium ion beam was used for comparison.

A reversed bias of 20, 40, 60, 80 or 100 V is applied at the diode. The IBIC intensity is normalized with the PIXE intensity in order to get rid of the influence of the ion beam fluctuation. IBIC is increased while the bias increase. It is because the Schottky barrier is getting wilder and more energy of the incident particles deposits in the depletion layer. Because the helium ion beam has higher stopping power in comparison with the proton beam, it produces more electron-hole pairs in the depletion layer. The IBIC image produced by helium ion beam has better contrast than that by proton beam. According to the thickness of the surface layer and the depletion layer of the chip, a proper species and energy of the incident particles can be selected in order to collect charges at certain depth of the semiconductor chip.

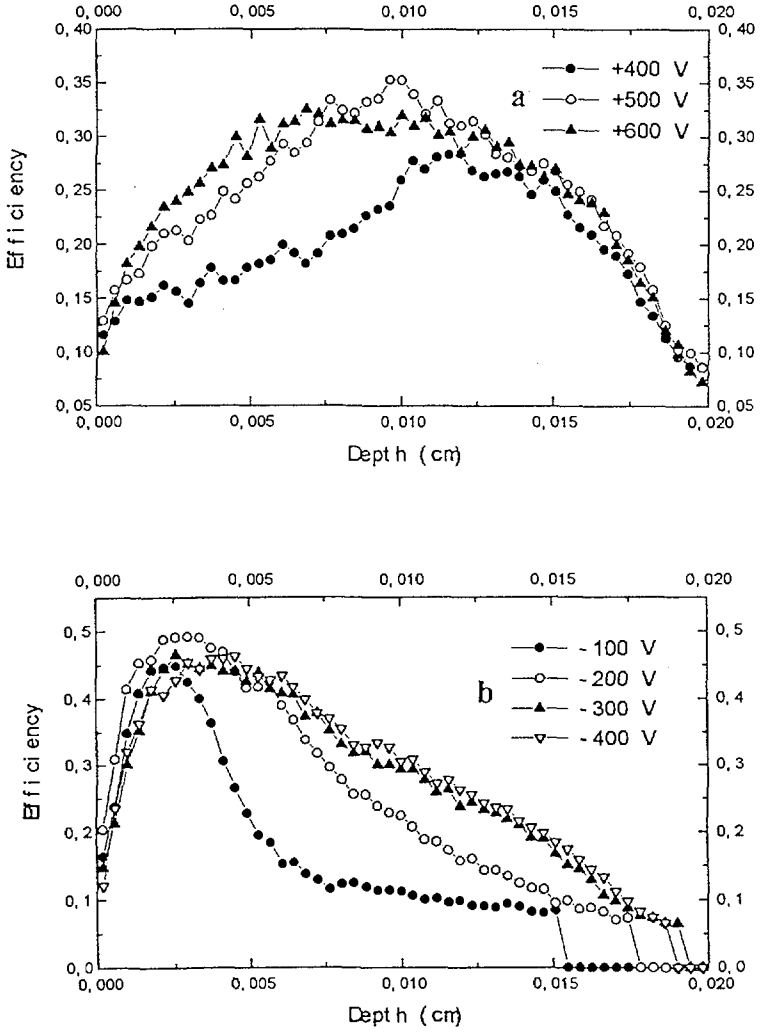

Fig. 7. Charge collection efficiency profile along the CVD diamond growth direction for positive bias (a) and negative bias (b). The growth side (biased) is on the left of the diagram.

5.4. Ion beam synthesis and analysis of combinatorial material chips (libraries)

The combinatorial approach has been widely used for the new drug discovery [5]. Combining the physical masks with thin film synthesis technique [6], integrated material chips (libraries) with a large number of spatially defined different compounds are generated. The combinatorial technique can be widely used in material science to increase the rate of new material discovery and optimization by several orders of magnitude.

During the last few years special interest has been devoted to create new nano-crystals of metals or compounds in SiO_2, which may exhibit specific optical emission properties and be interesting for photoelectric application. The ion implantation is attractive for this purpose. It generates nano-crystals with well-defined concentration at pre-calculated depths below the host material surface. Our first application of the combinatorial approach in ion implantation is intended to increase greatly the efficiency of sample synthesis and the possibility of novel nano-crystal formation, which may yield higher energy emission.

Although the application of combinatorial approach could revolutionize new material discovery, the in-depth study of the materials libraries is restricted by the difficulty in the phase determination and composition inhomogeneity examination of the small individual samples on the material chips. The electron beam induced cathodoluminescence (CL) technique contribute to the luminescent properties of the materials. The techniques of MeV ion beam Rutherford backscattering spectrometry (RBS) and proton elastic backscattering (PEB) are first applied for characterization of the

combinatorial material chips to determine the depth-resolved ion distribution in the implanted samples.

Boron (P-type) doped 0.5 mm thick single crystal silicon wafers were used for the implantation. SiO_2 thin film of ~ 400 nm was formed by thermal oxidation. Six ion species of C, Ga, N, Pb, Sn and Y were sequentially implanted to the SiO_2 film through combinatorial masks and consequently a library of 64 (2^6) samples is generated by 6 masking combinations. This approach offers rapid synthesis of samples with potential new compounds formed in the matrix. The generated materials chip was subsequently thermally annealed at 800 $^{\circ}$ C for 30 min in Ar gas. Fig. 8 shows the schematic of the combinatorial material chip holder for RBS and PEB analysis. The double arrow lines represent that the holder is controllably moved along X and Y directions to let the selected sample on the chip aligned with the analyzing beam.

RBS analysis was performed by using 2 MeV $^4He^+$ beam at a scattering angle of 170 $^{\circ}$. The spectra obtained by RBS measurements are partially shown in Fig. 9. Fig. 9(a) shows the spectra of the co-implanted samples S(Ga, N) and S(Ga, C). The Ga spectrum of S(Ga, N) is peaked at ~36 nm from the surface. Concerning the N depth range which is estimated to be peaked at ~130 nm from the surface, we can conclude that no GaN crystals formed. Two peaks of Ga spectrum for S(Ga, C) are revealed in Fig. 9(a), which indicates that the C existence induces the redistribution of Ga in SiO_2 after annealing. The profile for C distribution is peaked at ~180 nm from the surface, which matches the location of the lower energy peak of Ga spectrum (172 nm from the surface). It is expected that C induced Ga-related compounds may be formed in the SiO_2 film. Subsequent implantation of Pb or Pb + Sn into the S(Ga, C) samples did not alter the Ga spectrum peak location, as partially shown in Fig. 9(b). By comparing the spectra of S(Ga, Pb, N) and S(Ga, Pb, Sn, N) in Fig. 9(b), it shows that the interaction between Pb and Sn is little.

The previous discussion is also confirmed by the ion concentration depth-profiles calculated with RUMP program, which are shown in Fig. 10, corresponding to Fig. 9. The Ga profile of S(Ga, C) is peaked at 36 and 172 nm from the surface, with corresponding atom fractions of 1.5% and 0.56%, respectively (Fig. 10(a)). The profiling curves of S(Ga, Pb, C) and S(Ga, Pb, Sn, C) also each show two peaks of Ga concentration, located at nearly the same position as that of S(Ga, C). Fig, 10(b) reveals that Sn diffusion approaching the surface for S(Pb, Sn, N) is evident, which is a cause of higher energy luminescent emission when bombarding it with electron beam.

Fig.11 shows PEB spectra of S(C), S(N) and pristine SiO_2 by 3 MeV H^+ beams at a scattering angle of 170 $^{\circ}$. The peak concentration of C for S(C) is 4.12%, calculated using the proton elastic scattering cross section enhancement factors [7]. There is no N revealed in the spectrum of S(N). It is owing to the N diffusion and escaping out off SiO_2 during annealing. The PEB cross sections of light elements C, N and O are enhanced for proton energy > 2.5 MeV. Therefor, the profiling of these elements over a sufficient depth range in a heavy material can be readily accomplished.

We have successfully developed a combinatorial ion synthesis and ion beam analysis technique to study the ion-implanted combinatorial material chips (libraries). It greatly increases the efficiency of sample synthesis, analysis and optimization [8].

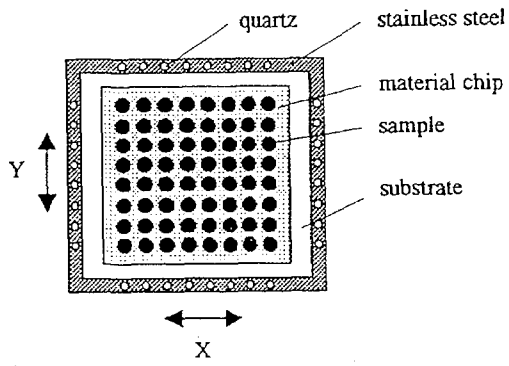

Fig. 8. Schematic of material chip holder for RBS and PEB analysis. The double arrow represent that the holder is able to move along X and Y directions to make the sample aligned with the analysing beam.

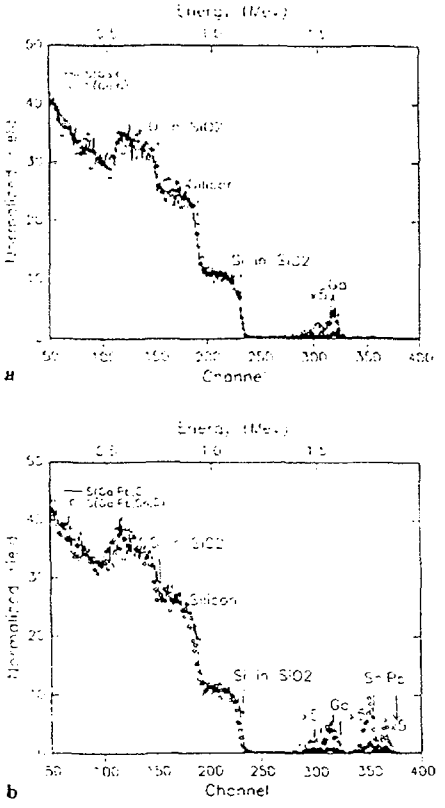

Fig. 9. 2.0 MeV $^4He^+$ RBS spectra from material chip after annealing at 8000°C for 30 min in Ar gas. (a) S(Ga, C) and S(Ga, N); (b) S(Ga, Pb, C) and S(Ga, Pb, Sn, C).

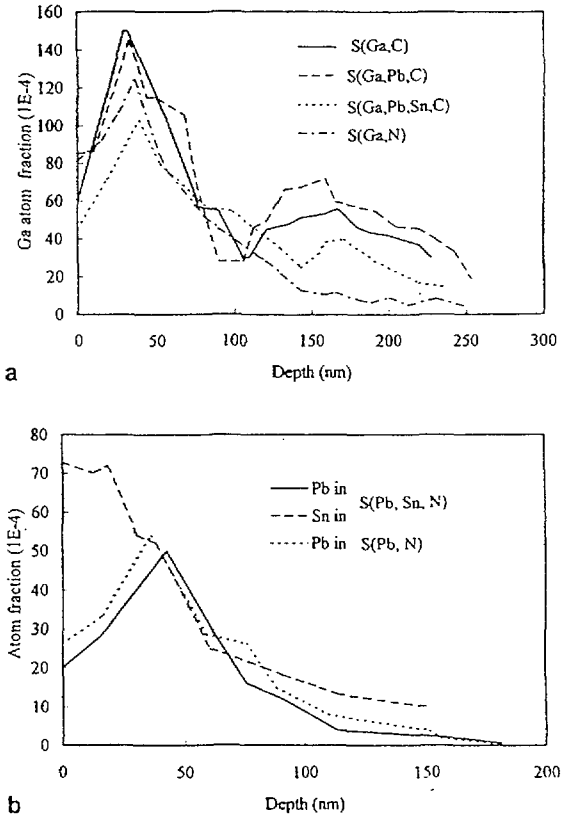

Fig. 10. Ion concentration depth profiles determined from the RBS measurements for the material chip. (a) Ga profiles for S(Ga, C), S(Ga, Pb, C), S(Ga, Pb, Sn, C) and S(Ga, N). (b) Profiles of Pb and Sn for S(Pb, Sn, N) in comparison with Pb profiles for S(Pb, N).

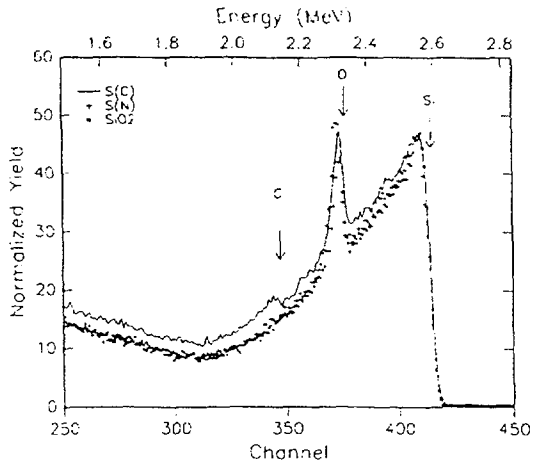

Fig. 11. Proton elastic backscattering spectra using 3.0 MeV H^+ on SiO_2, S(C) and S(N).

REFERENCES

[1] J. Shi , D. Jiang, S. Tan, J. Guo, Mater. Res. Bull, 26 (1991) 1277

[2] Z. Wang, J. Zhang, J. Pan, J. Mater. Sci. Lett. 13 (1994) 427

[3] G. N. Van Wyk, J. Du Plessis, E. Talauer, Surf. Sci. 254 (1991) 73

[4] R. Li, C. Li, W. Whang, Appl. Phys. A50 (1990) 169

[5] B. A. Bunin, M. J. Plunkett, J. A. Ellman, Proc. Natl. Acad. Sci. USA 91 (1994) 4708

[6] X. D. Xiang, X. D. Sun, G. Briceno, Y. Lou, K. A. Wang. H. Chang, W. G. Wallace-Freedman, S. W. Chen, P. G. Schultz, Science 268 (1995) 1739

[7] G. Yang, D. Zhu, H. Hu, H. Pan, Nucl. Instr. and Meth. B 61 (1991) 175

[8] X. Liu, Z. Feng, W. Lu, S. Shen, C. Chen, D. Zhu, J. Hu, M. Li, Appl. Phys. Lett. 1999 75 (17) 25